Measurement of surface topography and stiffness distribution on cross section of *Xenopus laevis* tailbud for estimation of mechanical environment in embryo

[1]Fumiaki Murakami, [2]Yoriko Ando, [3,4]Asuka Miyagi, [1]Shukei Sugita, [3,4]Naoto Ueno, *[1]Takeo Matsumoto

1. Biomechanics Laboratory, Department of Mechanical Engineering, Graduate School of Engineering, Nagoya Institute of Technology, Gokiso-cho, Showa-ku, Nagoya 466-8555, Japan

2. Biomechanics Laboratory, Department of Mechanical Science and Engineering, Graduate School of Engineering, Nagoya University, Furo-cho, Chikusa-ku, Nagoya 464-8603, Japan

3. Division for Morphogenesis, Department of Developmental Biology, National Institute for Basic Biology, 38 Nishigonaka, Myodaiji, Okazaki, Aichi 444-8585, Japan

4. Department of Basic Biology, School of life Science, The Graduate University of Advanced Studies (SOKENDAI), 38 Nishigonaka, Myodaiji, Okazaki, Aichi 444-8585, Japan

FM performed the experiments and data analysis. YA analyzed the data and drafted the manuscript. AM and NU conducted embryo preparation and consulted the handling. SS examined the experimental methods. TM planned and organized the whole experiments.

*Corresponding author
Present affiliation: Biomechanics Laboratory, Department of Mechanical Science and Engineering, Graduate School of Engineering, Nagoya University, Furo-cho, Chikusa-ku, Nagoya 464-8603, Japan
Email: takeo@nagoya-u.jp
TEL/FAX: +81-52-789-2721

Abstract

The stress distribution inside a *Xenopus laevis* tailbud embryo was estimated to examine the cause of the straightening and elongation. The embryos were cut in the middle, yielding a cross section perpendicular to the body axis. The section was not flat, owing to the residual stress relief. The stress needed to restore the flatness corresponded to the stress inside the embryo and was calculated using the surface topography and Young's-moduli in the section. We found the areas of the notochord (Nc), neural tube (NT), and abdominal tissue (AT) bulged in the cross section, which revealed that compressive forces acted in these tissues. The moduli of the Nc, NT, and AT were in the order of several thousand, hundred, and tens of pascals, respectively. In the Nc, the compressive force was largest and increased with the development, suggesting Nc playing a central role in the elongation. The bending moment generated by the AT was 10 times higher than that by the Nc in the early stages of the tailbud formation, and the two were similar in the latter stages, suggesting that the compressive force in the AT was the major cause of the straightening during the early stage. The straightening and elongation could be orchestrated by changes in the compressive forces acting on the Nc, NT, and AT over time. For the sake of simplicity, we calculated the compressive force only and neglected the tensile force. Thus, it should noted that the amount of the compressive force was somewhat overestimated.

Keywords

Biomechanics, Physical force, Residual stress, Strain, Young's modulus

Introduction

How cell movement and tissue rearrangement are organized with the spatial and temporal control to achieve morphogenesis and organ function has been a longstanding question in development biology. Although developmental biology has focused on genes and chemical factors in the past decades, recent studies have suggested that mechanical forces play significant roles and produce specific changes in gene expression and chemical signaling through the process of mechanotransduction in tissue morphogenesis and development (Wozniak & Chen, 2009, Mammoto & Ingber, 2010, Lecuit *et al.*, 2011, Zhang & Labouesse, 2012). For instance, in a mouse embryo, fluid flow triggers the initial left–right body plan symmetry-breaking event in the ventral node (Nonaka *et al.*, 2002). In spite of accumulating evidence, the role of physical forces that orchestrate cellular process in regulating embryogenesis remains an unsolved problem.

The relative position of the cells and tissues continuously change so that the cells and tissues are formed at the correct time and location to establish the proper body plan (Nieuwkoop & Faber, 1994), and it is reasonably expected that the stress and strain distributions inside the embryo change with the deformation (Davidson, 2011). To address how the force-involved process *in vivo* is coordinated within the embryo, the quantification of the mechanical environment is necessary. Several techniques—such as the stress-relaxation test, tensile test, and laser-ablation test—have been performed to estimate the mechanical environment in embryonic tissues, and such approaches provide insights into the effects of physical forces on the morphogenesis (Wozniak & Chen, 2009, Mammoto & Ingber, 2010, Zhang & Labouesse, 2012). However, thus far, because of the technical difficulties, most of these techniques have been performed using embryonic tissue explants or on the surface of embryos.

In this study, we investigated the stress and strain distributions inside the *Xenopus* tailbud embryo to examine the relationship between the morphogenesis and the mechanical environment. The tailbud embryo deformed from a curved rounded shape resembling a kidney to a straight elongated shape along the anterior–posterior (AP) axis. The tailbud embryo had stiffer tissue than the earlier-stage embryos, and its deformation was far simpler than that occurring during gastrulation. Thus, compared with the earlier-stage embryos, it was easier to measure the mechanical properties of the tailbud embryo and discuss the effects of physical forces. To estimate the stress distribution inside the embryo, the deformation of the tissue due to stress relief upon cutting was utilized (Figure 1). When an elastic body with residual stress was sectioned, a dent appeared on the section where the tensile residual stress was applied before the

sectioning, owing to the stress relief in the vicinity of the cut surface. Similarly, a bulge appeared in the area with compressive residual stress (Matsumoto *et al.*, 2004). The amount of stress needed to restore the flatness of the section corresponds to the residual stress inside the embryo. To determine the residual stress at a point on the section, we needed to measure the strain and Young's modulus at the point. The strain was estimated by measuring the surface topography of the sections using a three-dimensional (3D) laser scanning confocal microscope. The Young's modulus was measured using an indentation tester developed in our laboratory for this purpose. According to the strain and Young's-modulus distributions on the cross-section perpendicular to the AP axis, the temporal change in the mechanical environment inside the embryo in the tailbud stage was estimated.

Materials and methods

Embryos

Xenopus laevis embryos were obtained via standard methods (Morita *et al.*, 2010) and cultured in 1× Steinberg's solution at 12–13 °C until stage (St.) 22–24 (Nieuwkoop & Faber, 1994).

Embryo sectioning

The tailbud embryo was mounted in low-gelling temperature (30–31 °C) agar (1%, Nacalai Tesque, Kyoto, Japan), and the agar was trimmed to form a cuboid with dimensions of approximately 4 × 4 × 5 mm (Fig. 2). The experimental setup for the embryo sectioning and the surface-topography measurement is shown in Fig. 2. The agar block containing the embryo was attached to the bottom of an acrylic bath (90 × 145 × 15 mm) using double-stick tape to keep the AP axis of the embryo vertical. Then, a float (approximately 5 × 5 × 6 mm block of a formed sterol weighing 3 mg) was pasted at the top of the block using an adhesive. Using this float, the upper half of the block was removed immediately after sectioning to minimize the re-adhesion of the cut surfaces, allowing the surface-topography measurement to be started seconds after the sectioning. The bath was placed on the stage of a shape-measurement laser microscope (VK-X105, Keyence, Osaka, Japan) and filled with 0.1× Steinberg's solution to cover the sample. To cut the embryo, a Micro Cautery Instrument (MC-2010, Protech International, TX, USA) was used. The embryo in the agar block was cut using an electrified platinum wire (PT-351075, Nilaco, Tokyo, Japan) having a diameter of 20 μm stretched at the tip of the electrode. The position of the electrode was adjusted using a 3D manipulator to cut the embryo

in half, lengthwise. The motorized stage of the microscope was moved in the horizontal direction to cut the embryo with a speed of 10 mm/s and stopped when the sample reached the position directly under the objective lens.

Surface-topography measurement

The surface topography of the cross section of the embryo was measured using a shape-measurement laser microscope with a 5× objective lens (CF IC EPI Plan 5×A, Nikon, Tokyo, Japan) whose tip was covered with a laboratory-made lens cover resembling a swimming goggle, as the objective was not a water-immersion type (Fig. 2). Bright-field images of the section were obtained using a color charge-coupled device (CCD) camera equipped in the microscope. A preliminary study revealed bulges at the notochord (Nc), neural tube (NT), and abdominal tissue (AT) on the cross section; thus, we focused on these three tissues in subsequent measurements. We identified these areas by carefully comparing the bright-field, laser-intensity, and surface-topography images (see Fig. 5 for example) and determined the regions of interest (ROIs) in each area, as shown in Fig. 3 (the regions surrounded by the white broken lines). Identification was performed by a single experienced researcher (FM) with the aid of image processing techniques, i.e., by adjusting the black and white balance and/or sharpness of these images. The midline of the embryo was drawn by connecting the ventral and dorsal ends on the section (blue line in Fig. 3). We then drew a straight line in each area that passed through the highest point of that area and was perpendicular to the midline (red lines in Fig. 3), and the height distribution along this line was obtained. According to the obtained height distribution, the protrusion of each area, H was calculated by subtracting the average height outside the ROI from that within the ROI. The cross-sectional area of each ROI was also calculated.

Indentation test and calculation of Young's modulus

We developed an indentation tester to measure the stiffness on the cross section of the embryo for specimens prepared similarly to those for the surface-topography measurement and obtained the Young's moduli of the Nc, NT, and AT. Figure 4(a) shows the setup of the indentation tester. The indentation was formed by a glass indenter with a tip diameter of approximately 60 μm attached to the tip of a cantilever made of polyethylene terephthalate (PET) film with a Young's

modulus of 4.2 GPa (27077, A-one, 3M Japan, Tokyo, Japan), as shown in Fig. 4(b). Two cantilevers with different spring constants—0.026 and 0.016 N/m—were used to cover the measurement range of several pascals to kilopascals. Figure 4(c) shows the method used to measure the amount of indentation d and the deflection of the cantilever δ during the indentation test. The shape-measurement laser microscope was used to monitor the height of the cantilever tip. The height was determined by observing the intensity of the laser reflection from the cantilever surface using a 40× water-immersion objective lens. First, the indenter was placed directly above the embryo using a three-axis manipulator (MHW-3, Narishige, Japan) as shown in Fig. 4(a). Next, the stage was raised to bring the indenter into contact with the sample. The contact was indicated by the cessation of the vibration of the indenter. The position of the cantilever at the time of contact was defined as the reference. The cantilever root was then lowered by 10 μm using the three-axis manipulator (Fig. 4(a)), and the height of the indenter was measured again by lowering the objective until a clear, focused image of the indenter was obtained. The displacement of the objective corresponded to the indentation d. The deflection of the cantilever was obtained as $\delta = z - d$, where z denotes the total displacement of the cantilever root. We repeated this process 10–15 times to obtain the d–δ relationship. Because the wound-healing response occurred after the cutting of the tailbud embryo and the epidermal tissue eventually occluded the cross section, it was sometimes difficult to perform the indentation test multiple times for the same embryo. The indentation test was thus performed in one area for each embryo.

The Young's modulus was obtained from the force curve, i.e., the relationship between the amount of indentation d and the indentation force F. The force was calculated by multiplying the deflection of the cantilever d by its spring constant k: $F = k\delta$. The d–F relationship was fitted using Eq. 1, which is derived from Hertz's elastic contact theory:

$$F = \frac{4Er^{1/2}d^{3/2}}{3\left(1-\nu^2\right)}, \tag{1}$$

where d is the amount of indentation into the embryonic tissue, r is the radius of the indenter, E is the Young's modulus of the embryo, and ν the Poisson's ratio. We assumed the incompressibility of the embryonic tissue and set ν as 0.5. In a preliminary study, we performed the indentation test on 0.6w/v% agar gel to determine its Young's modulus and compared this

value with the modulus obtained in the uniaxial compression test of the same sample. The difference was <22%, confirming that the indentation tester yielded an accurate value.

Estimation of mechanical environment in embryonic tissues

The stress and strain in the embryonic tissues were estimated as those necessary to restore the bumpy cut surface to a flat plane. As the first step of the estimation, the following assumptions were made: 1) the embryo was composed of four types of tissues, i.e., Nc, NT, AT, and other tissues; 2) each tissue was homogeneous, isotropic, and incompressible; and 3) each tissue behaved elastically with the Young's modulus obtained in the indentation test. The average stress and strain were determined for each tissue according to the amount of protrusion H and the Young's modulus E of each type of tissue. The strain is generally defined as

$$\varepsilon = \frac{L - L_0}{L_0} = \frac{\Delta L}{L_0}, \tag{2}$$

where L is the length after deformation, L_0 is the initial length, and ΔL is the deformed length of the sample. In this study, ΔL was considered as the protrusion of each tissue measured in the previous section, and L_0 was the depth of the zone where the surface deformation caused strain. According to Saint–Venant's Principle, this depth corresponds to the diameter D of the tissue if each tissue is assumed to be cylindrical for simplicity (Fig. 1). The diameter D of each tissue was calculated using the cross-sectional area S, as follows:

$$D = 2\sqrt{\frac{S}{\pi}}. \tag{3}$$

The strain in each tissue was thus obtained as

$$\varepsilon = \frac{H}{D}, \tag{4}$$

and the stress σ in each tissue was obtained as

$$\sigma = \varepsilon E. \tag{5}$$

Because the deformation that occurred during the tailbud stage involved not only elongation of the tissue along the body axis but also the straightening of the axis, we evaluated the moment of force M in the embryo to investigate the effects of the force exerted by the tissues on the straightening. For this, we needed the force F generated by each tissue and its moment arm l, i.e., the distance from the center of the cross section. The force F generated by each tissue inside the embryo was calculated by multiplying the stress σ by the cross-sectional area S:

$$F = \sigma S . \tag{6}$$

Because the Nc was located very close to the center of the cross section, we selected the Nc as the reference point for the moment of force. The moment arm l was thus calculated as the distance between the centroids of Nc and NT or AT. The moment of force was obtained as

$$M = Fl \tag{7}$$

for NT and AT. The parameters S and l were measured on the cross section of the embryos using the image-processing software ImageJ (NIH).

Results

Surface topography

Figure 5 shows a bright-field image (left), a laser-intensity image with the region of the tissues marked (center), and a height-distribution image (right) of the cross sections of embryos at St. 26, 31, and 35–36. The hole near the center of each section is the cavity of the intestinal tract. The Nc and AT protruded from the surrounding tissues at all stages. Figure 6 summarizes the changes in the protrusions in the three areas during the development of the embryo. A Dunnet's multiple test with a significance level of 0.05 against St. 24 was performed using KaleidaGraph v. 4.1 (Synergy Software, PA, USA). There was no significant difference in the Nc. On the other hand, there were significant differences in the NT at St. 33–34 and 35–36 and in the AT at St. 32 and 35–36 with respect to St. 24. Analysis of the correlation between the protrusion and the stage revealed a positive correlation (R = 0.49) in the NT and a negative correlation (R = −0.49) in the AT. These results indicate that the protrusion of the NT and AT tended to increase and decrease, respectively, with the development of the embryo.

Stiffness of cross section of tailbud embryo

The Young's moduli for the Nc, NT, and AT of the embryo at St. 26, 31, and 35–36 were calculated, as shown in Fig. 7. The Young's moduli of the Nc, NT, and AT were equal to several kilopascals, several hundreds of pascals, and several tens of pascals, respectively, during this period, exhibiting a significant difference between the tissues. The Young's modulus of the Nc was significantly higher at St. 35–36 than at St. 26. Although the Young's modulus did not differ significantly between St. 26 and 31 and between St. 31 and 35–36, it tended to increase with the

development of the embryo. In the NT, no significant difference was observed between the stages, and there was no change in the Young's modulus with the development of the embryo. In the AT, the Young's modulus was significantly smaller at St. 31 than at St. 26. Apart from this, no significant difference was observed between the stages.

Estimation of mechanical environment in tailbud embryo

Figures 8 and 9 show the residual stress and the force, respectively, generated by each tissue in the AP-axis direction at St. 26, 31, and 35–36. The Young's moduli averaged for each tissue at each stage (Fig. 7) were used for estimation. The strain of each tissue was calculated according to the amount of protrusion (Fig. 6) and the cross-sectional area of the sample. It is desirable to perform the surface-topography measurement and the indentation tests of all three tissues in the same embryo. However, because the deformation of the cross section possibly due to wound-healing response started just after the cutting of the tailbud embryo and epidermal tissue eventually occluded the cross section, it was difficult to do so. The residual stresses were thus estimated by using the mean values of the Young's modulus of each tissue. For the Nc, there was a significant difference between St. 26, 31 and St. 26, 35–36 for the stress and the force, both of which tended to increase with the development of the embryo. For the NT, there was a significant difference between all the stages in the stress and between St. 26, 35–36 and St. 31, 35–36 in force, and there was a tendency for both to increase. On the other hand, for the AT, there was a significant difference between St. 26, 31 and St. 26, 35–36 in both the stress and the force. Unlike the Nc and NT, the AT decreased with the development of the embryo.

The moments of force around the centroid of the Nc generated by the NT and AT were calculated at St. 26 (in the middle of the early tailbud stage) and at St. 35–36 (in the middle of the late tailbud stage), as shown in Fig. 10. At St. 26, the moment generated by the AT was almost 10 times higher than that for the NT, but at St. 35–36, there was no significant difference between them. The values of the parameters, protrusion, cross-section, diameter, Young's modulus, moment arm, which were used for the estimation of mechanical environment at stage 26, 31, and 35-36 are listed in Supplemental Table 1.

Discussion

We examined the stress distribution inside the *Xenopus* tailbud embryo to address the relationship between the morphogenesis and the mechanical environment. To determine the

residual stress, we measured the surface topography and the Young's-modulus distribution on the cross section of the tailbud embryo. The measurement of the surface topography of the cross section of the tailbud revealed that the Nc, NT, and AT bulged prominently. These tissues underwent compressive stress inside the embryo, which is considered to be the cause of the deformation and elongation in the AP-axis direction. Next, we developed an indentation tester to measure the Young's modulus of the cross-section of the tailbud embryo. At St. 26, 31, and 35–36, the Young's moduli of the Nc, NT, and AT were equal to several kilopascals, several hundred pascals, and several tens of pascals, respectively, indicating a significant difference between the tissues. This indicates that measurement of the surface topography is not sufficient to estimate the residual stress in the body; thus, the tissue stiffness must be measured. The Young's modulus of the Nc was the highest among the tissues. The Young's modulus calculated according to the bending stiffness, diameter, and length of the Nc at St. 26 by Adams et al. (Adams *et al.*, 1990) was approximately 5.3 kPa, which is consistent with our measurement. There is support for and against a mechanical role of the notochord in dorsal elongation and straightening in the early embryo stages. A study reported that the notochord is involved in elongation of the embryo because the embryonic body failed to elongate in any region where the notochord had been removed (Kitchin, 1949). In contrast, some other studies insisted that the mechanical role of the notochord is insignificant because embryos without notochords could elongate nearly as well as those with notochord (Malacinski & Youn, 1981, Zhou *et al.*, 2009) in the neural tailbud stages. During the post-neural tailbud stages, however, there have been no studies questioning the mechanical roles of the notochord to the authors' knowledge. It has been suggested that the notochord may function in elongation and straightening of the embryo (Kitchin, 1949, Mookerjee, 1953) and as a structural support (Bruns & Gross, 1970). The highest stiffness and stiffening observed in our measurement may be beneficial in the development process during the tailbud stages. As the stress is obtained by multiplying the strain by the Young's modulus of the tissue, the stress and the Young's modulus are closely related. The contribution of the actin-based cytoskeleton to the tissue stiffness and elastic modulus has been reported (Nagayama *et al.*, 2006, Zhou *et al.*, 2009, Harris & Charras, 2011). Therefore, the effect of the cytoskeleton on the mechanical environment in the embryo will be obtained by examining the time-dependent change of the mechanical properties of the tissue and the cytoskeletal element that induced stress in the tissue.

The residual stresses and the forces generated by the tissues were compressive and tended to increase in the Nc and NT and decrease in the AT during the tailbud stages of the

embryo development. This suggests that in the early tailbud stage, the Nc and AT bore the compressive force and thus extended the embryo body in the AP-axis direction, whereas in the latter stage, the Nc and NT did so. The moments of force in the NT and AT around the centroids of the Nc were calculated, and their effects on the morphogenesis were examined. At St. 26, the moment of the AT was almost 10 times higher than that of the NT, but at St. 35–36, there was no significant difference between them. The tailbud embryonic stages are divided into early stages (St. 22–28) and late stages (St. 29–44). In the early stages, the embryo deforms from a curved shape to a straight shape and is simultaneously elongated in the AP-axis direction. In the late stages, it is further elongated in this direction (Nieuwkoop & Faber, 1994). The higher moment in the AT in the early stages may have caused the straightening of the embryonic body, and the balanced moment in the late stages may have been the driving force that extended the body without bending (Figure 11).

In this study, we estimated the residual stress in the embryo—to our knowledge, for the first time—by measuring the surface topography and the stiffness distribution in the cross section of the embryo, i.e., the tissue protrusion used in the present study contains not only the amount of bulge but also that of dent, and is somewhat larger than the amount of the bulge alone. We thus need to pay attention that the mechanical parameters obtained in this study is the estimation of the maximum values. The relationship between the mechanical factor and the morphogenesis was examined. However, we evaluated only the compressive stress estimated according to the bulged areas of the cross section of the embryo. In a future study, we need to estimate the tensile stress by measuring the Young's modulus in the dented areas. The strain was estimated according to Saint–Venant's Principle. The strain in a body calculated using this method is valid only when the shape of the body is the same in the depth-wise direction, e.g., a cylinder and is embedded in a semi-finite parent phase. We must employ finite-element analysis to estimate the stress and strain distributions in the embryo. Because severing an embryo is a non-physiological treatment, it is desirable to measure the stress distribution in a more non-invasive manner. In recent years, the real-time observation of the movement inside the embryo via magnetic resonance imaging and X-rays has been reported (Papan *et al.*, 2007, Moosmann *et al.*, 2013). Using the information regarding the tissue location and movement obtained from these studies and the mechanical properties of the tissue, simulations such as the finite-element method will make it possible to address specially and temporally regulated embryonic mechanics.

Acknowledgements

This work was supported in part by Grants-in-Aid for Scientific Research on Innovative Areas (3218-22127008 and 3705-15H05860) from MEXT.

References

Adams, D. S., Keller, R. & Koehl, M. a. R. 1990. The Mechanics of Notochord Elongation, Straightening and Stiffening in the Embryo of Xenopus-Laevis. *Development,* **110,** 115-130.

Bruns, R. R. & Gross, J. 1970. Studies on the tadpole tail. I. Structure and organization of the notochord and its covering layers in Rana catesbeiana. *Am J Anat,* **128,** 193-233.

Davidson, L. A. 2011. Embryo mechanics: balancing force production with elastic resistance during morphogenesis. *Curr Top Dev Biol,* **95,** 215-241.

Harris, A. R. & Charras, G. T. 2011. Experimental validation of atomic force microscopy-based cell elasticity measurements. *Nanotechnology,* **22,** 345102.

Kitchin, I. C. 1949. The effects of notochordectomy in Amblystoma mexicanum. *J Exp Zool,* **112,** 393-415.

Lecuit, T., Lenne, P. F. & Munro, E. 2011. Force generation, transmission, and integration during cell and tissue morphogenesis. *Annu Rev Cell Dev Biol,* **27,** 157-184.

Malacinski, G. M. & Youn, B. W. 1981. Neural plate morphogenesis and axial stretching in "notochord-defective" Xenopus laevis embryos. *Dev Biol,* **88,** 352-357.

Mammoto, T. & Ingber, D. E. 2010. Mechanical control of tissue and organ development. *Development,* **137,** 1407-1420.

Matsumoto, T., Goto, T., Furukawa, T. & Sato, M. 2004. Residual stress and strain in the lamellar unit of the porcine aorta: experiment and analysis. *Journal of Biomechanics,* **37,** 807-815.

Mookerjee, S. 1953. An Experimental Study of the Development of the Notochordal Sheath. *J. Embryol. exp. Morph.,* **1,** 411-416.

Moosmann, J., Ershov, A., Altapova, V. et al. 2013. X-ray phase-contrast in vivo microtomography probes new aspects of Xenopus gastrulation. *Nature,* **497,** 374-377.

Morita, H., Nandadasa, S., Yamamoto, T. S., Terasaka-Iioka, C., Wylie, C. & Ueno, N. 2010. Nectin-2 and N-cadherin interact through extracellular domains and induce apical accumulation of F-actin in apical constriction of Xenopus neural tube morphogenesis. *Development,* **137,** 1315-1325.

Nagayama, K., Nagano, Y., Sato, M. & Matsumoto, T. 2006. Effect of actin filament distribution on tensile properties of smooth muscle cells obtained from rat thoracic aortas. *Journal of Biomechanics,* **39,** 293–301.

Nieuwkoop, P. D. & Faber, J. 1994. *Normal Table of Xenopus laevis (Daudin).* Garland Publishing Inc.

Nonaka, S., Shiratori, H., Saijoh, Y. & Hamada, H. 2002. Determination of left-right patterning of the mouse embryo by artificial nodal flow. *Nature,* **418,** 96-99.

Papan, C., Boulat, B., Velan, S. S., Fraser, S. E. & Jacobs, R. E. 2007. Formation of the dorsal marginal zone in Xenopus laevis analyzed by time-lapse microscopic magnetic resonance imaging. *Developmental Biology,* **305,** 161-171.

Wozniak, M. A. & Chen, C. S. 2009. Mechanotransduction in development: a growing role for contractility. *Nat Rev Mol Cell Biol,* **10,** 34-43.

Zhang, H. M. & Labouesse, M. 2012. Signalling through mechanical inputs - a coordinated process. *Journal of Cell Science,* **125,** 3039-3049.

Zhou, J., Kim, H. Y. & Davidson, L. A. 2009. Actomyosin stiffens the vertebrate embryo during crucial stages of elongation and neural tube closure. *Development,* **136,** 677-688.

Figure legends

Figure 1. Schema of the residual stress estimation method used in the present study. If the tissue (a) elongates spontaneously, compressive stress (blue) appears in this tissue and a tensile stress (red) appears in the rest of the tissue (b) as a reaction. Upon sectioning, a bulge appears in the tissue (a) and the tissue (b) shrinks due to the release of the residual stress. According to Saint-Venant's Principle, the depth of the zone where the residual stress in the tissue (a) becomes negligibly small corresponds to the diameter *D* of the tissue. *H*, amount of protrusion; *D*, diameter of a tissue; ε, strain; *E*, Young's modulus; σ, stress; F, force.

Figure 2. Experimental setup for the embryo sectioning and the surface-topography measurement. The inset shows a tailbud embryo mounted in agarose gel.

Figure 3. Laser-intensity image of a *Xenopus laevis* tailbud embryo. D, dorsal; V, ventral. The scale bar represents 500 μm.

Figure 4. Schematics of the indentation tester (a), the glass indenter (b), and the measurement principle of the amount of indentation and the deflection of the cantilever (c).

Figure 5. Bright-field images (left), laser-intensity images (middle) and topography images (right) of the cross-section of *Xenopus laevis* tailbud embryos at St. 26 (upper panels), 31 (middle panels), and St. 35–36 (lower panels). NT, Neural tube; Nc, notochord; AT, abdominal tissue. The scale bar represents 500 μm.

Figure 6. Protrusion of the Nc, NT, and AT on the cross-section of *Xenopus laevis* tailbud embryos from St. 24 to 35–36. Scale bar = 500 μm.

Figure 7. Young's moduli of the Nc (a), NT (b), and AT (c) on the cross-section of *Xenopus laevis* tailbud embryos at St. 26, 31, and 35–36.

Figure 8. Residual stress in the AP-axis direction in the Nc (a), NT (b), and AT (c) of *Xenopus laevis* tailbud embryos at St. 26, 31, and 35–36.

Figure 9. Force in the AP-axis direction in the Nc (a), NT (b), and AT (c) of *Xenopus laevis* tailbud embryos at St. 26, 31, and 35–36.

Figure 10. Moment of force around the centroid of the Nc in the tailbud embryo stage.

Figure 11. Schema of tailbud deformation driven by compressive forces generated by the AT, Nc, and NT. (a) In its early stage (top), the moment of force generated by the AT is dominant and this causes straightening of the tailbud. (b) In its late stage (bottom), the moment of forces generated by AT and NT balance and the sum of compressive forces *F* generated by the AT, Nc, and NT increases, causing the elongation in the body axis instead of the straightening. M, moment, *F*, force; *l*, moment arm; D, dorsal; V, ventral; A, anterior; P, posterior. The scale bar represents 1 mm.

Supplemental Table 1. The values of the parameters, protrusion, cross-section, diameter, Young's modulus, moment arm, which were used for the estimation of mechanical environment at stage 26, 31, and 35-36.

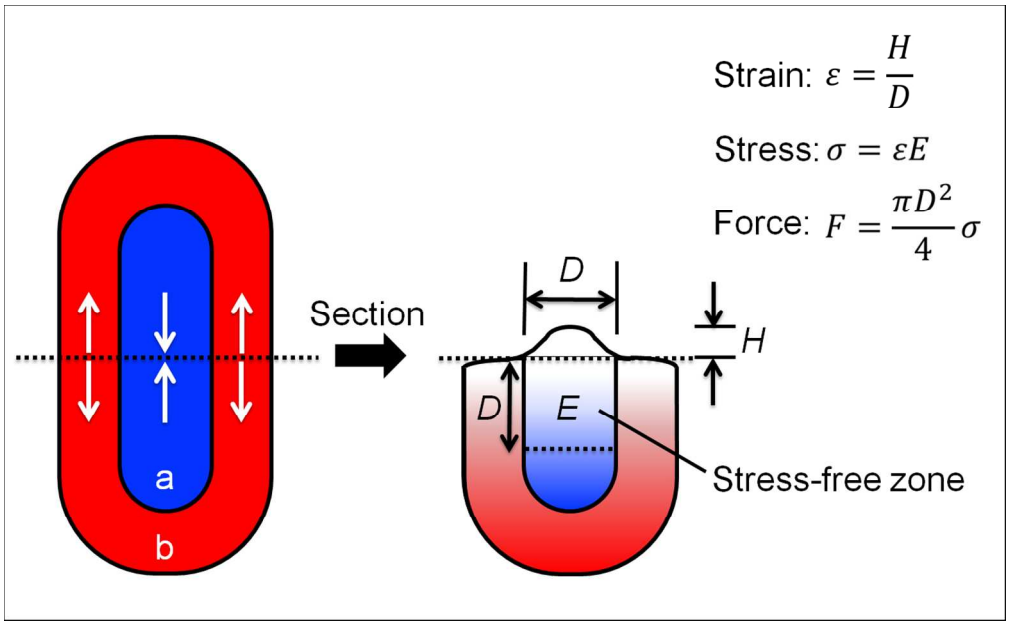

Figure 1. Schema of the residual stress estimation method used in the present study. If the tissue (a) elongates spontaneously, compressive stress (blue) appears in this tissue and a tensile stress (red) appears in the rest of the tissue (b) as a reaction. Upon sectioning, a bulge appears in the tissue (a) and the tissue (b) shrinks due to the release of the residual stress. According to Saint-Venant's Principle, the depth of the zone where the residual stress in the tissue (a) becomes negligibly small corresponds to the diameter D of the tissue. H, amount of protrusion; D, diameter of a tissue; ε, strain; E, Young's modulus; σ, stress; F, force.

244x150mm (150 x 150 DPI)

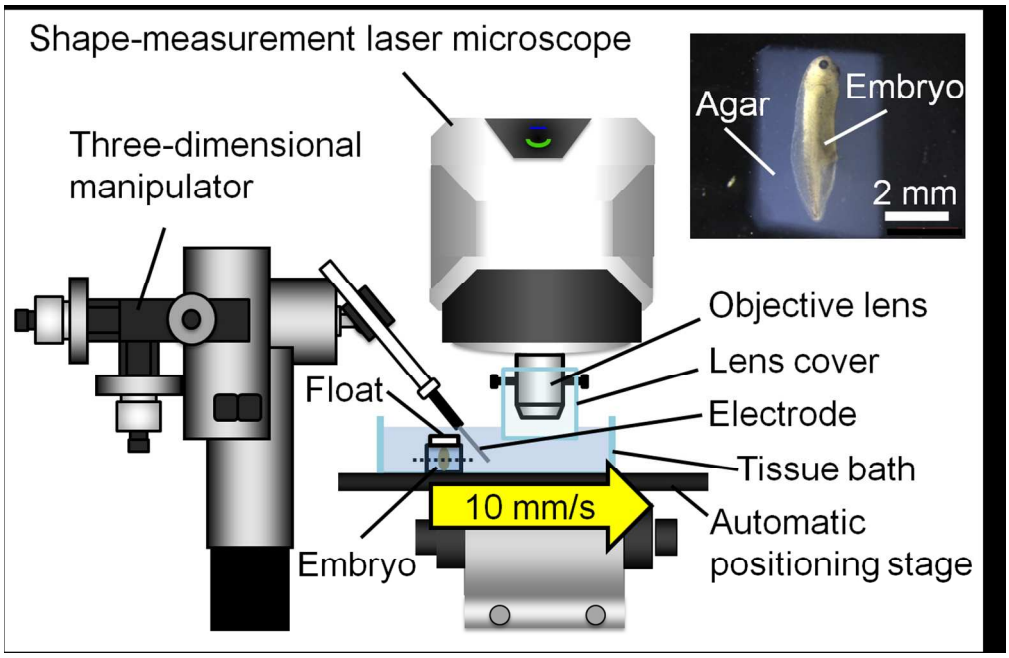

Figure 2. Experimental setup for the embryo sectioning and the surface-topography measurement. The inset shows a tailbud embryo mounted in agarose gel.

241x155mm (150 x 150 DPI)

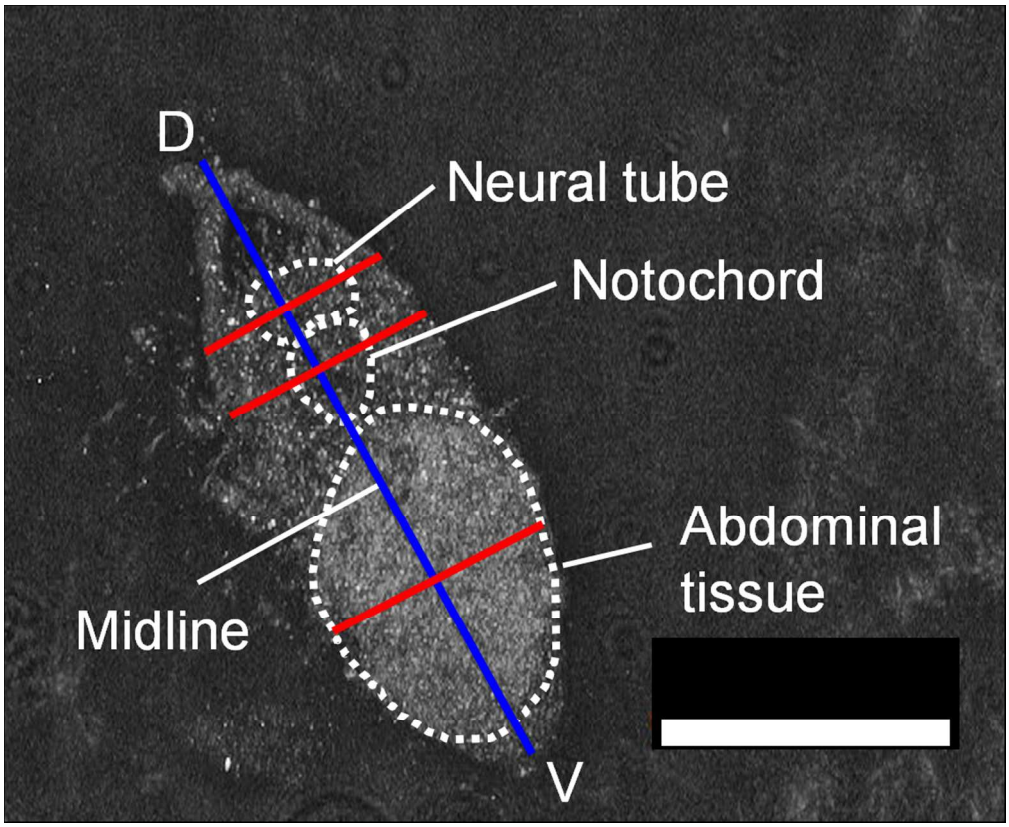

Figure 3. Laser-intensity image of a Xenopus laevis tailbud embryo. D, dorsal; V, ventral. The scale bar represents 500 μm.

192x157mm (150 x 150 DPI)

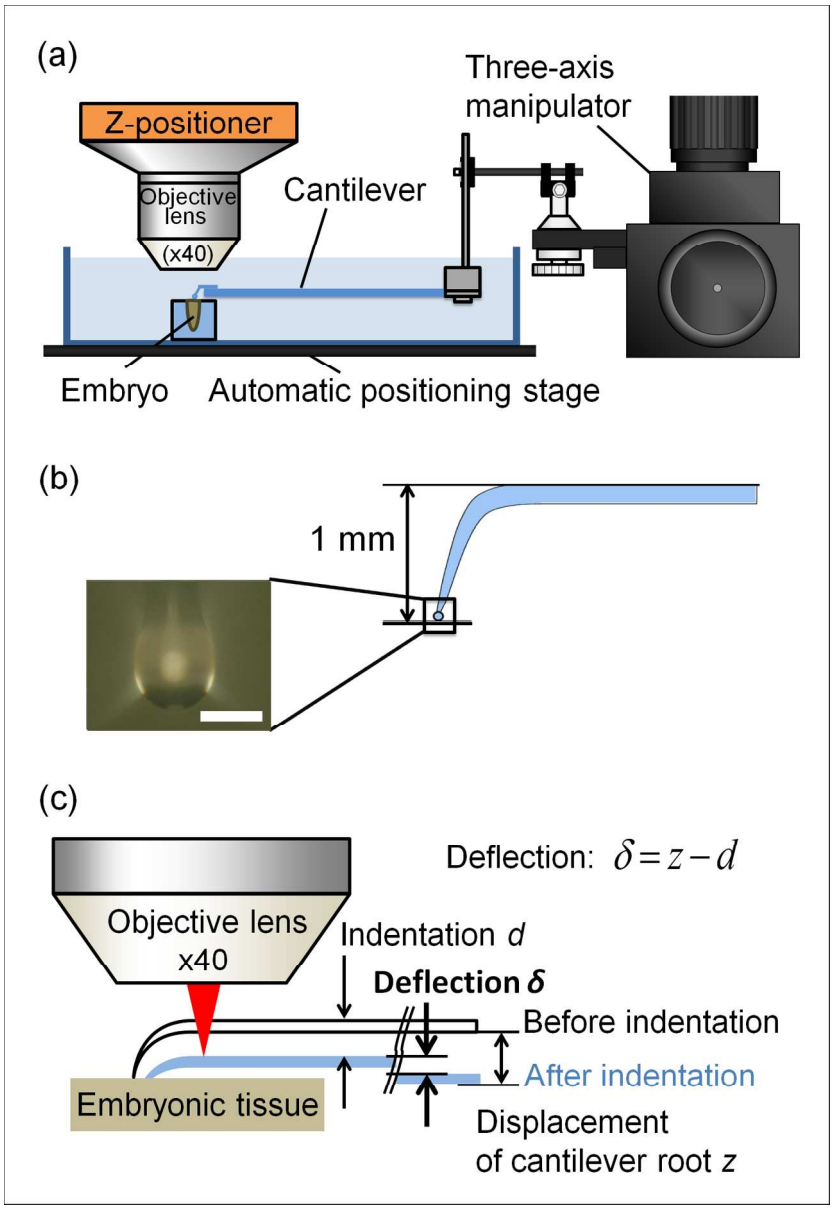

Figure 4. Schematics of the indentation tester (a), the glass indenter (b), and the measurement principle of the amount of indentation and the deflection of the cantilever (c).

254x370mm (150 x 150 DPI)

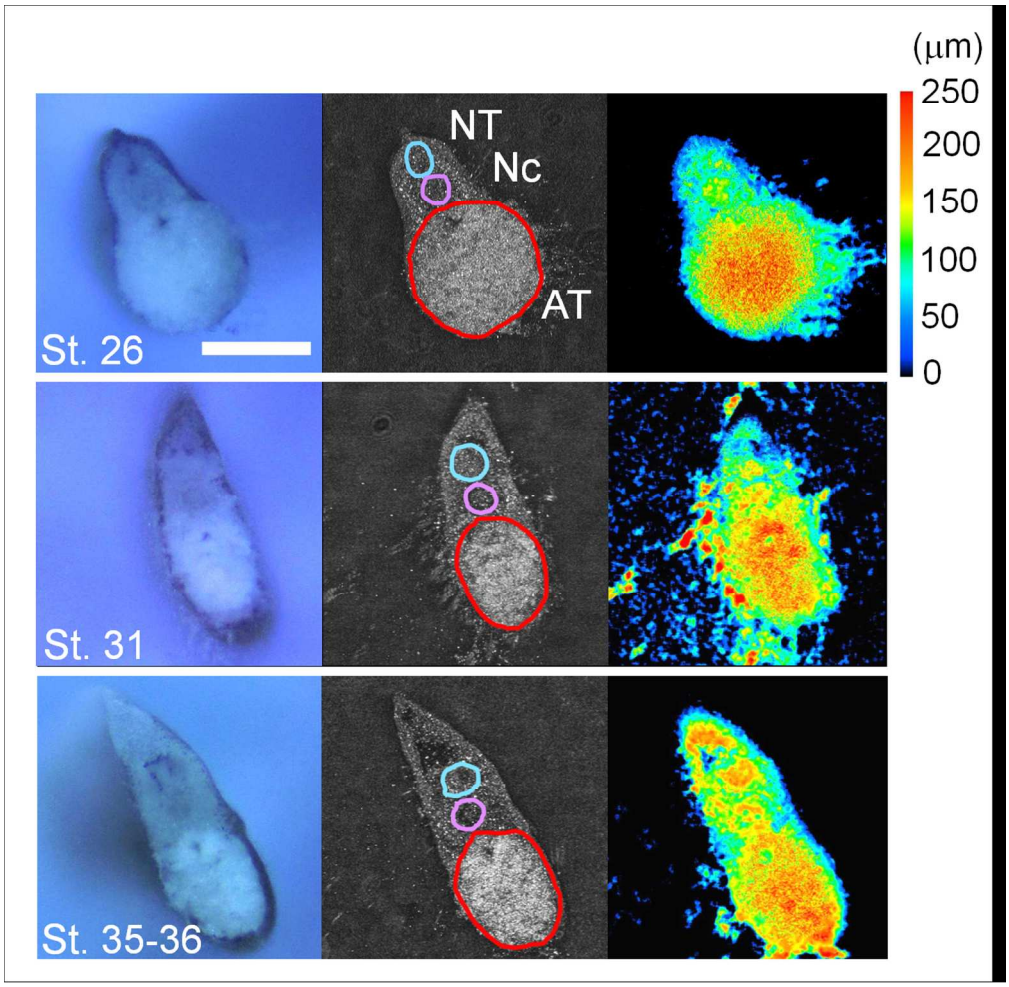

Figure 5. Bright-field images (left), laser-intensity images (middle) and topography images (right) of the cross-section of Xenopus laevis tailbud embryos at St. 26 (upper panels), 31 (middle panels), and St. 35–36 (lower panels). NT, Neural tube; Nc, notochord; AT, abdominal tissue. The scale bar represents 500 μμm.

243x237mm (150 x 150 DPI)

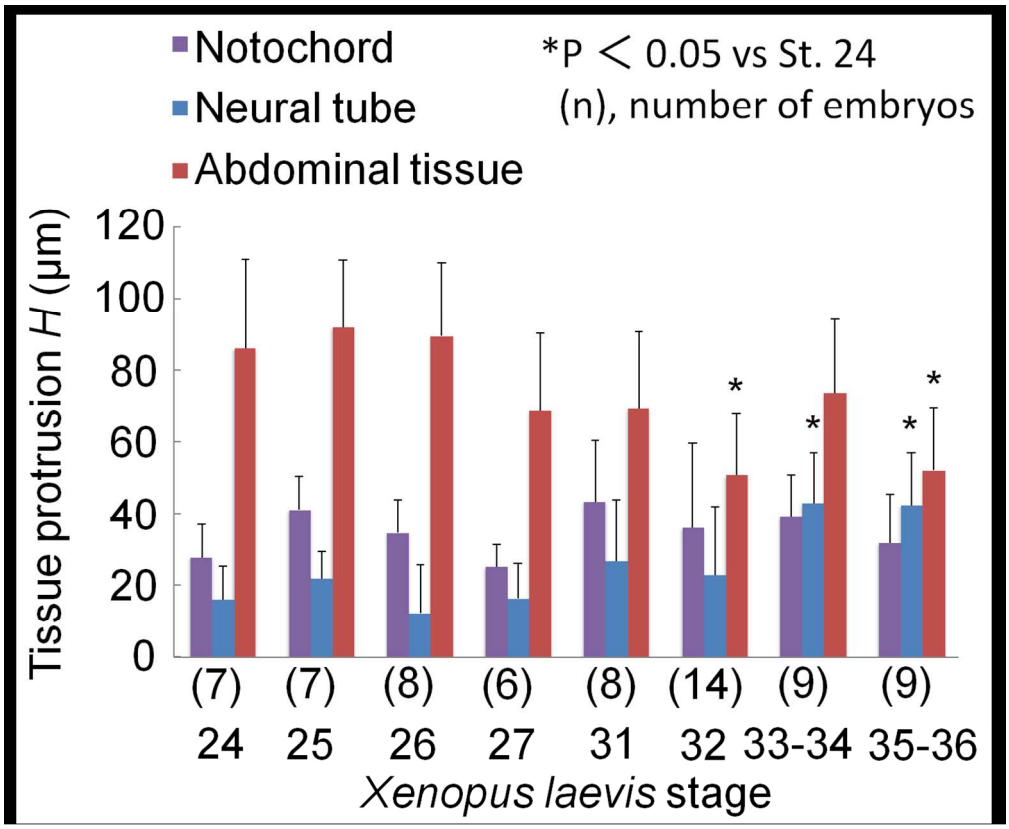

Figure 6. Protrusion of the Nc, NT, and AT on the cross-section of Xenopus laevis tailbud embryos from St. 24 to 35–36. Scale bar = 500 μμm.

245x200mm (150 x 150 DPI)

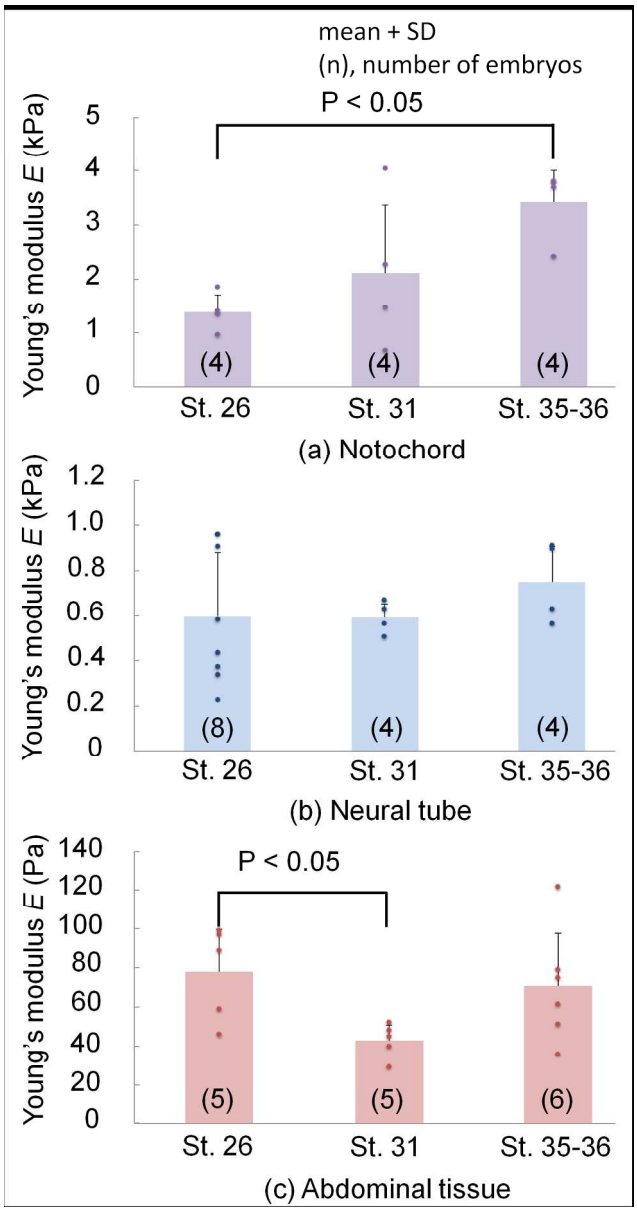

Figure 7. Young's moduli of the Nc (a), NT (b), and AT (c) on the cross-section of Xenopus laevis tailbud embryos at St. 26, 31, and 35–36.

242x462mm (150 x 150 DPI)

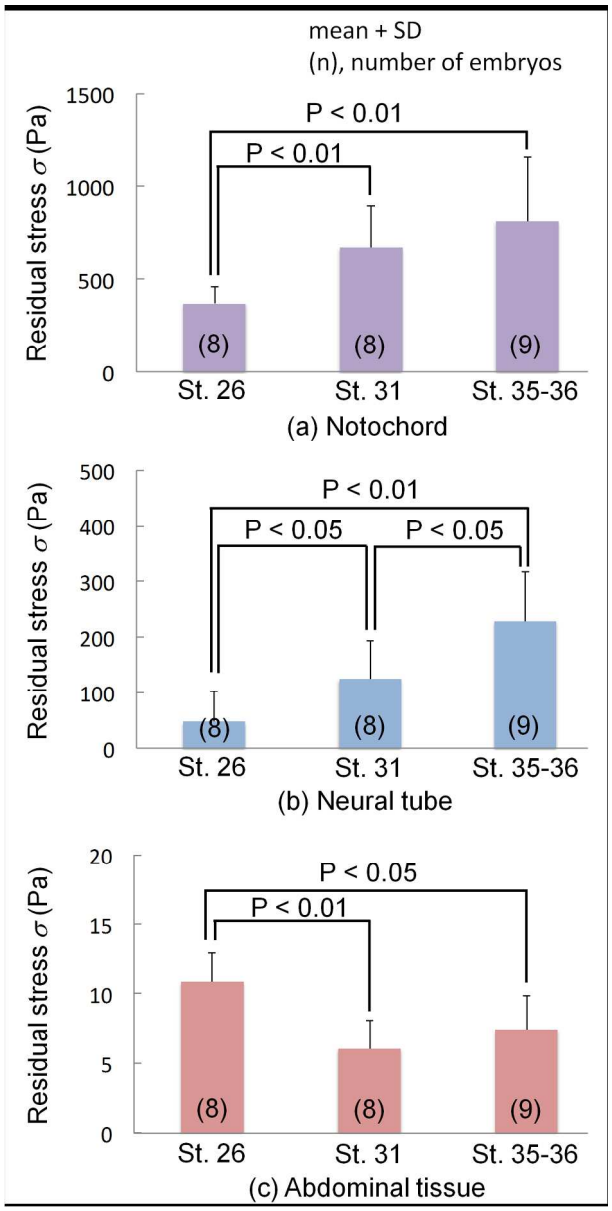

Figure 8. Residual stress in the AP-axis direction in the Nc (a), NT (b), and AT (c) of Xenopus laevis tailbud embryos at St. 26, 31, and 35–36.

242x483mm (150 x 150 DPI)

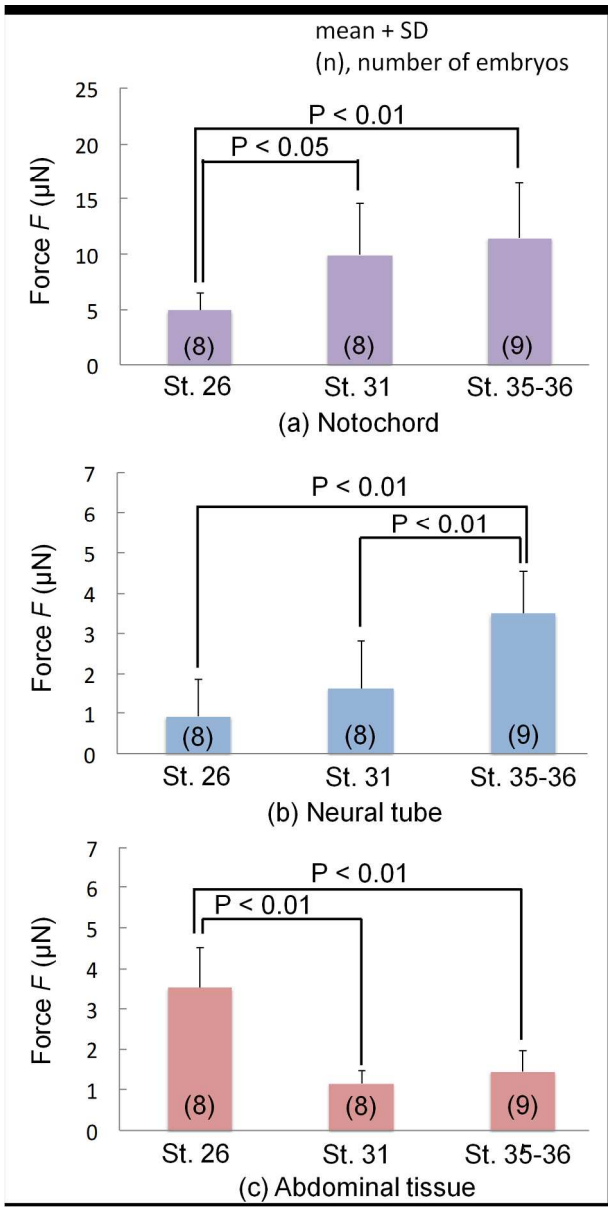

Figure 9. Force in the AP-axis direction in the Nc (a), NT (b), and AT (c) of Xenopus laevis tailbud embryos at St. 26, 31, and 35–36.

242x482mm (150 x 150 DPI)

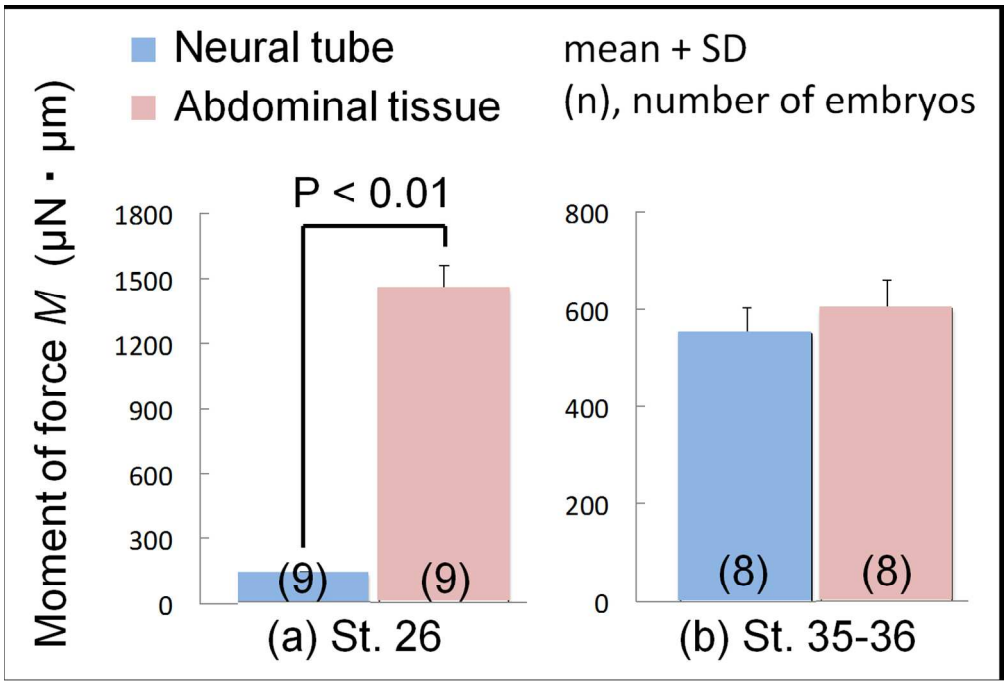

Figure 10. Moment of force around the centroid of the Nc in the tailbud embryo stage.

246x166mm (150 x 150 DPI)

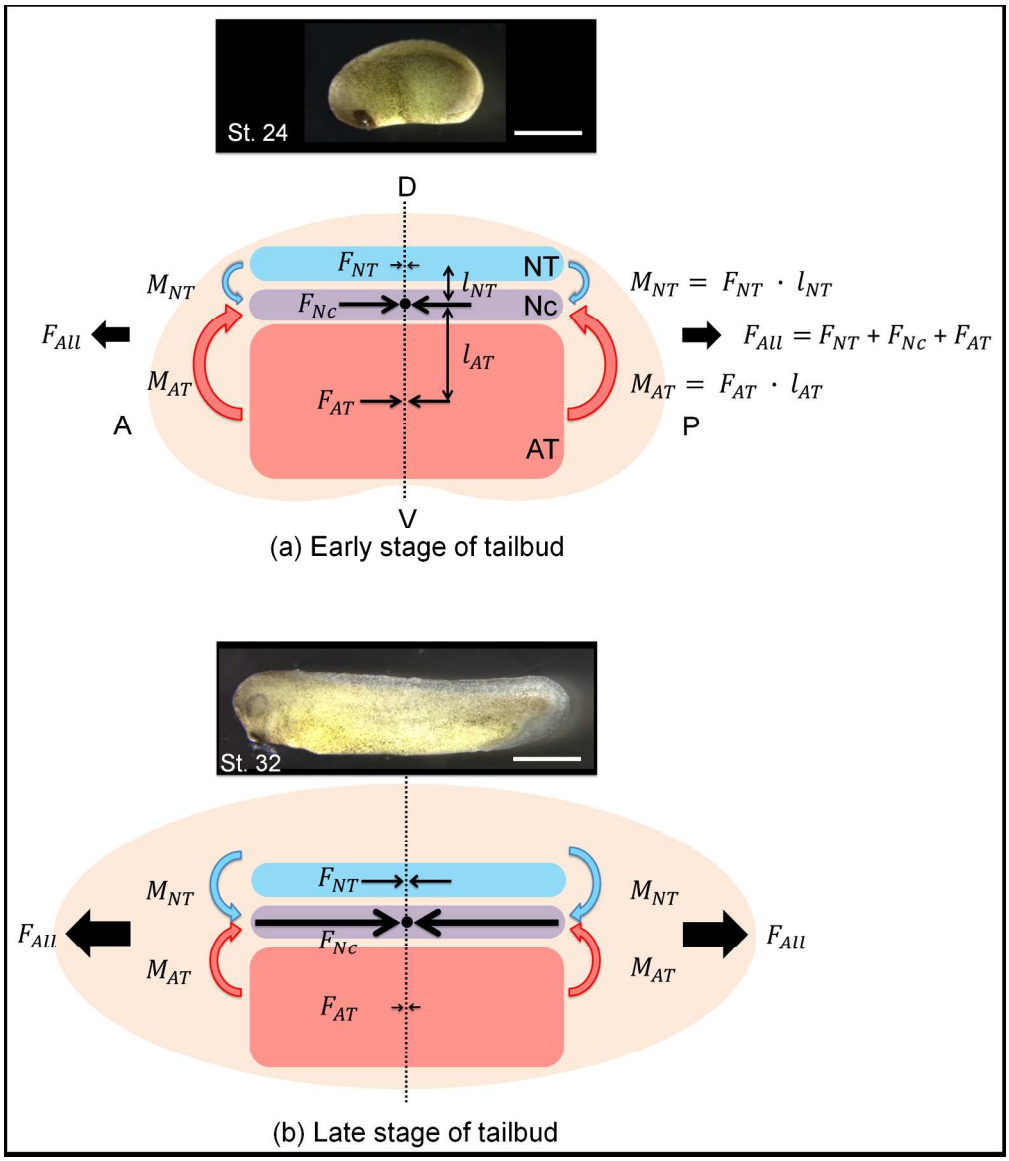

Figure 11. Schema of tailbud deformation driven by compressive forces generated by the AT, Nc, and NT. (a) In its early stage (top), the moment of force generated by the AT is dominant and this causes straightening of the tailbud. (b) In its late stage (bottom), the moment of forces generated by AT and NT balance and the sum of compressive forces F generated by the AT, Nc, and NT increases, causing the elongation in the body axis instead of the straightening. M, moment, F, force; l, moment arm; D, dorsal; V, ventral; A, anterior; P, posterior. The scale bar represents 1 mm.

414x476mm (150 x 150 DPI)

Supplemental Table 1. The values of the parameters, protrusion, cross-section, diameter, Young's modulus, moment arm, which were used for the estimation of mechanical environment at stage 26, 31, and 35-36.

(mean ± SD, *n* in the parentheses)

	Protrusion (μm)	Cross-section ($\times 10^4$ μm^2)	Diameter (μm)	Young's modulus (Pa)	Arm length from notochord (μm)
			Stage 26		
Nc	34.6±9.1 (8)	1.33±0.26 (8)	129.7±12.4 (8)	1390.0 (4)	—
NT	12.4±13.3 (8)	2.04±0.31 (8)	160.6±12.2 (8)	598.3 (8)	143.9±11.0 (8)
AT	89.4±20.6 (8)	32.3±3.87 (8)	640.2±39.3 (8)	78.0 (5)	409.5±31.0 (8)
			Stage 31		
Nc	43.2±17.1 (8)	1.44±0.37 (8)	134.8±16.7 (8)	2116.9 (4)	—
NT	26.7±17.2 (8)	1.23±0.34 (8)	124.0±18.6 (8)	593.0 (4)	—
AT	69.3±21.2 (8)	19.6±2.89 (8)	498.3±35.1 (8)	42.7 (5)	—
			Stage 35-36		
Nc	31.7±13.7 (9)	1.45±0.17 (9)	135.6±8.0 (9)	3428.4 (4)	—
NT	42.2±14.7 (9)	1.57±0.19 (9)	141.3±8.3 (9)	752.1 (4)	158.3±15.6 (9)
AT	52.0±17.6 (9)	19.4±2.57 (9)	495.7±33.0 (9)	70.8 (6)	415.7±42.5 (9)

Nc, notochord; NT, neural tube; AT, abdominal tissue.